OPEN ACCESS
JOURNAL OF ADVANCED DIELECTRICS
Vol. 11, No. 4 (2021) 2150018 (9 pages)

DOI: 10.1142/S2010135X21500181

High energy storage density with ultra-high efficiency and fast charging–discharging capability of sodium bismuth niobate lead-free ceramics

Abdul Manan*,‖, Maqbool Ur Rehman*, Atta Ullah†, Arbab Safeer Ahmad†,
Yaseen Iqbal‡, Ibrahim Qazi§, Murad Ali Khan*,
Hidayat Ullah Shah* and Arshad Hussain Wazir¶

*Laboratory for Research in Advanced Materials, Department of Physics
University of Science and Technology Bannu, Township Bannu
28100 Khyber Pakhtunkhwa, Pakistan

†Center for Material Science, Islamia College Peshawar
Peshawar, 25120 Khyber Pakhtunkhwa, Pakistan

‡Materials Research Laboratory, Department of Physics
University of Peshawar, 25120 KP, Pakistan

§Department of Materials Science and Engineering, Institute of Space Technology
Islamabad, 44000 Islamabad, Pakistan

¶Department of Chemistry, University of Science and Technology Bannu
28100 Khyber Pakhtunkhwa, Pakistan

‖drmanan82@yahoo.com

Received 25 March 2021; Revised 17 April 2021; Accepted 3 June 2021; Published 8 July 2021

Ceramics-based capacitors with excellent energy storage characteristics, fast charging/discharge rate, and high efficiency have received significant attention. In this work, $Na_{0.73}Bi_{0.09}NbO_3$ (NBN) ceramics were processed through solid-state sintering route. The investigated ceramics were crystallized in a single perovskite phase. Dense microstructure, with small average grain size (~0.92 μm) is obtained for the investigated ceramics. A high dielectric constant >1000 accompanied by a low dielectric loss was achieved for these ceramics at ambient temperature. A recoverable energy density ~0.92 J/cm^3 and ultra-high efficiency of 96.33% at 138 kV/cm were obtained at room temperature. Furthermore, a lower discharging time of 0.14 μs was also achieved. This material is a suitable candidate for power pulsed applications.

Keywords: Polarization; energy density; capacitor; efficiency.

1. Introduction

Increased utilization of renewable energy requires improvement in advanced dielectric capacitors' efficiency and energy storage characteristics to broaden its application area. Ceramic dielectric capacitors possess high dielectric constant, fast charging and discharging capabilities, long life cycle, and good mechanical and thermal stabilities at high-temperatures.[1–4] The critical parameters by which the dielectric ceramics are evaluated for energy storage capability include high charged energy density (W_s), high recoverable energy density (W_{rec}), a high efficiency (η), and a low discharge rate. The parameters' values are computed from the respective polarization versus electric field curve, i.e., the P–E loop via the following equations.[5–7]:

$$W_s = \int_0^{P_{max}} EdP, \tag{1}$$

$$W_{rec} = \int_{P_r}^{P_{max}} EdP, \tag{2}$$

$$\eta = \frac{W_{rec}}{W_s} \times 100. \tag{3}$$

Here, P_{max} demonstrates the extreme (maximum) polarization, P_r the remnant polarization, and E the electric field.

Figure 1 displays the schematic polarization versus electric field (P–E) loops of pure $NaNbO_3$ (NN) and partial Bi-substituted NN ceramics. This shows that partial Bi substitution for Na leads to slim polarization versus electric field (P–E) loop.

In the past, some linear dielectric materials such as mica and TiO_2 had been reported to exhibit very high efficiency; however, their very low dielectric constant restricted further increase in their energy storage density.[8–11] Therefore,

‖Corresponding author.

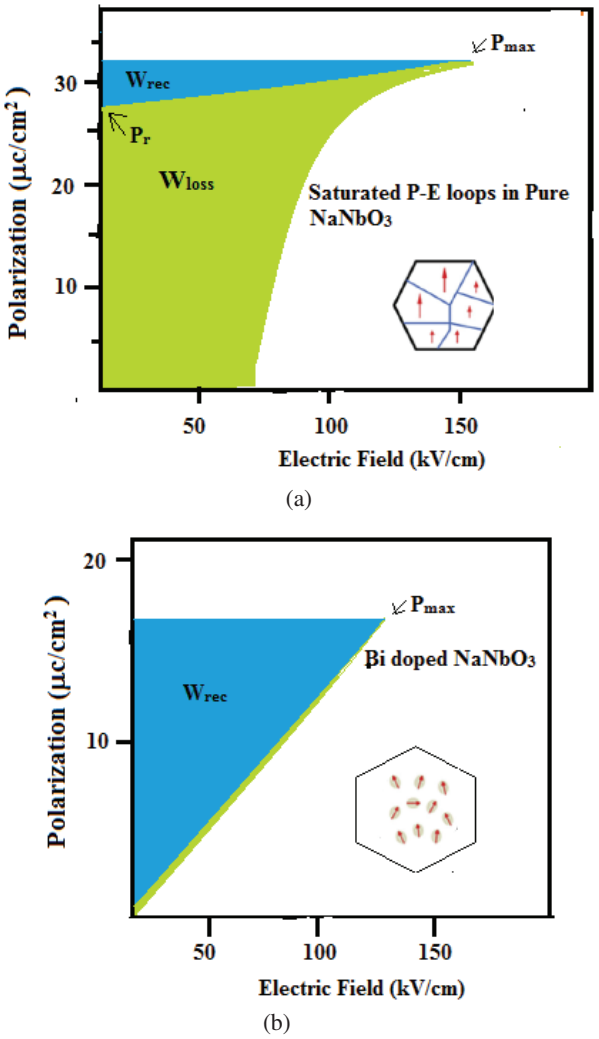

Fig. 1. Schematic of the polarization versus electric field (P–E) loops of (a) pure $NaNbO_3$ (NN) and (b) Bi-substituted NN ceramics.

nonlinear dielectrics, such as antiferroelectrics (AFEs) and relaxor ferroelectrics (RFEs) are being investigated for their energy storage characteristics as these materials possess extensive lattice polarization results with a high dielectric constant.[12–16] AFEs have anti-parallel adjacent dipoles leading to a zero net polarization. These materials exhibit high W_s due to a double hysteresis loop. Moreover, AFEs possess some drawbacks, e.g., first, AFEs usually have low breakdown strength (~10 kV/mm). Second, due to the large hysteresis of AFEs, energy is mostly wasted as heat energy, leading to a decrease in efficiency, usually less than 80%. It increases the material's temperature due to thermal destruction.[17,18]

On the other hand, RFEs have a lack of long-range order of dipoles resulting in low remnant polarization (P_r) and low coercive field (E_c), causing slanted and slim P–E hysteresis loops.[19,20] These materials also possess low dielectric loss allowing these to be suitable candidate materials for high energy density applications.[21] The relaxor maintains a relatively high dielectric polarization difference ($\Delta P = P_{max} - P_r$), resulting in high W_{rec} and high efficiency.[22]

Lead-free RFEs systems such as $BaTiO_3$ (BT)-based,[23–26] $K_{0.5}Na_{0.5}NbO_3$(KNN)-based,[27–30] $AgNbO_3$-based,[31–34] $BiFeO_3$-based,[21,35–38] $Bi_{0.5}Na_{0.5}TiO_3$ (BNT)-based,[39,40] have been investigated for their energy storage potential. KNN-based dielectrics are reported to possess $W_{rec} \sim 4$ J/cm^3 but with low η values (<65%).[29] However, the enhancement in energy storage characteristics still lags in that it is very difficult to get a high recoverable/discharge energy density (W_{rec}) and a high efficiency (η) simultaneously for a single material.

On the other hand, $NaNbO_3$ (NN) has been investigated due to its good piezoelectric properties. NN is known to exhibit a relatively lower theoretical density (4.55 g/cm^3), thus enabling light weight dielectric storage capacitors. Single crystal NN has been reported to possess AFE structure,[41] but its polycrystalline form displays a ferroelectric (FE) nature.[42,43] NN displays coexistence of FE P21ma (Q) and AFE Pbma (P) phases at room temperature. It is an easy way to enhance energy storage characteristics of NN-based materials via inducing relaxor characteristics through substitutions of suitable cations at the A site and/or B site of its perovskite structure. For example, Liu *et al.*, obtained a $W_{rec} \sim 0.55$ J/cm^3 and $\eta \sim 63\%$ for $NaNbO_3$–$CaZrO_3$ system.[44] Similarly, in another study, a W_{rec} of 2.20 J/cm^3 and η of 82% were reported for the $(1-x)$-$NaNbO_3$–$Bi(Zn_{0.5}Ti_{0.5})O_3$ ($x = 0.09$) ceramic system.[45] For the $0.90NaNbO_3$–$0.06BaZrO_3$–$0.04CaZrO_3$ ceramic system, a W_{rec} of 1.59 J/cm^3 and $\eta \sim 30\%$ were obtained.[46] Bismuth-containing lead-free relaxors have been investigated for high energy density capacitor applications in recent years.[47–52]

Therefore, the energy storage characteristics of $Na_{0.73}Bi_{0.09}NbO_3$ (NBN) ceramics were investigated for pulsed power applications in this study.

2. Experimental

NBN ceramics were fabricated through a solid-state mix oxide sintering process. Na_2CO_3 (99.9%, Alladin China), Bi_2O_3 (99%, Alladin China), Nb_2O_5 (99.9%, Alladin China) were used as the initial ingredients. These materials were weighed in stoichiometric ratio sand milling in isopropanol for 24 h with zirconia grinding balls to make a slurry. The slurry was dried at 95 °C in an electric oven overnight and then calcined for 2 h at 850 °C followed by re-ball milling for 24 h to get fine powders. The dried calcined powders were added with 5 wt% of PVA liquid solution as a binder and then grinded and sieved. The sieved powders were uniaxially pressed to make these pellets at a pressure of 100 MPa in a 12 mm diameter steel die using a hydraulic pellet press. These pellets were initially heated at 600 °C for two hours to expel the binder and finally sintered at 1275 °C for two hours. The phase constitution of the sintered samples was investigated using X-ray powder diffraction (XRD) with CuKα radiation (Bruker AXS D4 Endeavor).

The dense samples' surfaces were finely polished and etched thermally at 1150°C for 30 min, and Au coated for

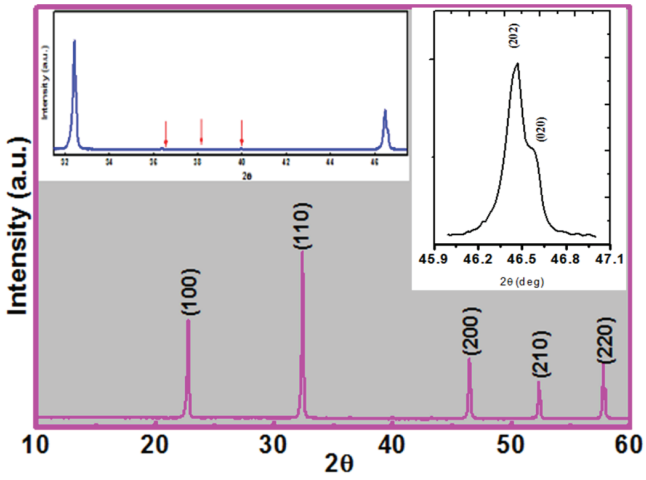

Fig. 2. XRD pattern of NBN ceramic recorded at room temperature, showing single perovskite phase crystallized into orthorhombic structure.

microstructural examination. For this purpose, a field emission scanning electron microscope (FESEM) (Jeol JXA 840A, Japan) was used.

To measure the dielectric characteristics, the opposite faces of ~0.7 mm thick sintered pellet was polished followed by silver pasting and heating at 800 °C for two hours. The dielectric loss (tanδ) and dielectric constant (ε_r) of these samples were determined in the temperature range of 20–500 °C at 1 kHz, 10 kHz, 100 kHz, and 1 MHz via a computer coupled LCR meter (E4980A, Agilent made of USA).

The electric field-dependent polarization at 1 Hz for a silver pasted 0.3 mm thick, dense sample by a dielectric test system (model Premier II, Radiant, USA) at different electric fields up to its dielectric breakdown strength (DBS). The composition's charging and discharging rates were tested with the help of a charge-discharge test system (model CPR1701–100, Ploy K) at an electric field of 43 kV/cm, 65 kV/cm, 87 kV/cm, and 108 kV/cm respectively.

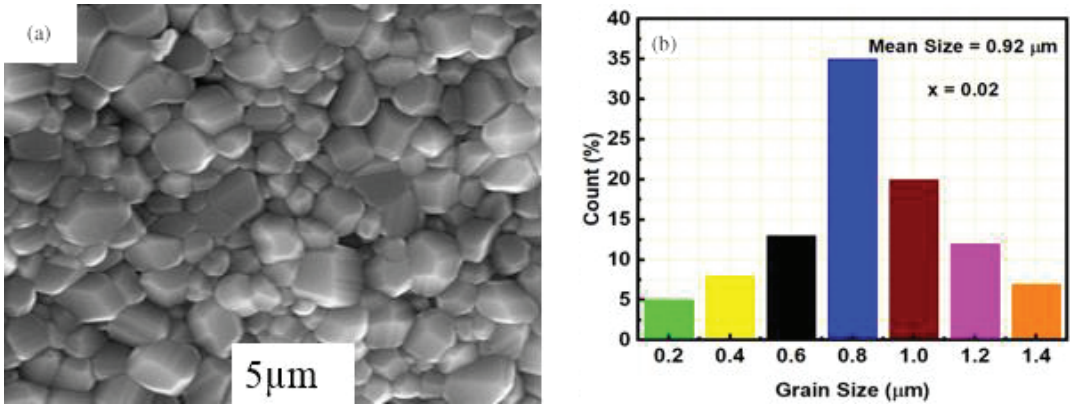

Fig. 3. (a) Scanning electron microscope image (SEM) and (b) the grain size distribution of NBN ceramics sintered at 1275 °C for two hours.

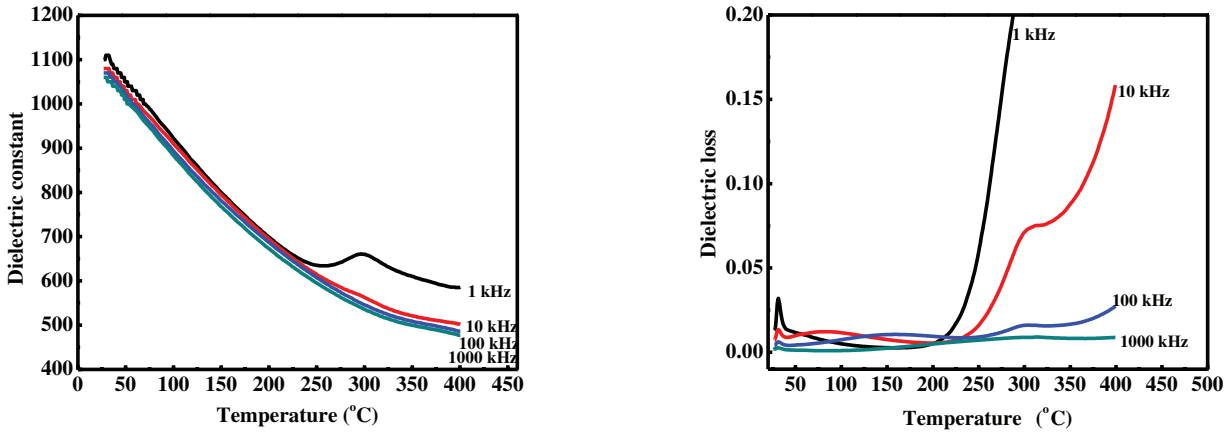

(a) (b)

Fig. 4. Variation in (a) ε_r and (b) tan δ of NBN ceramics with temperature.

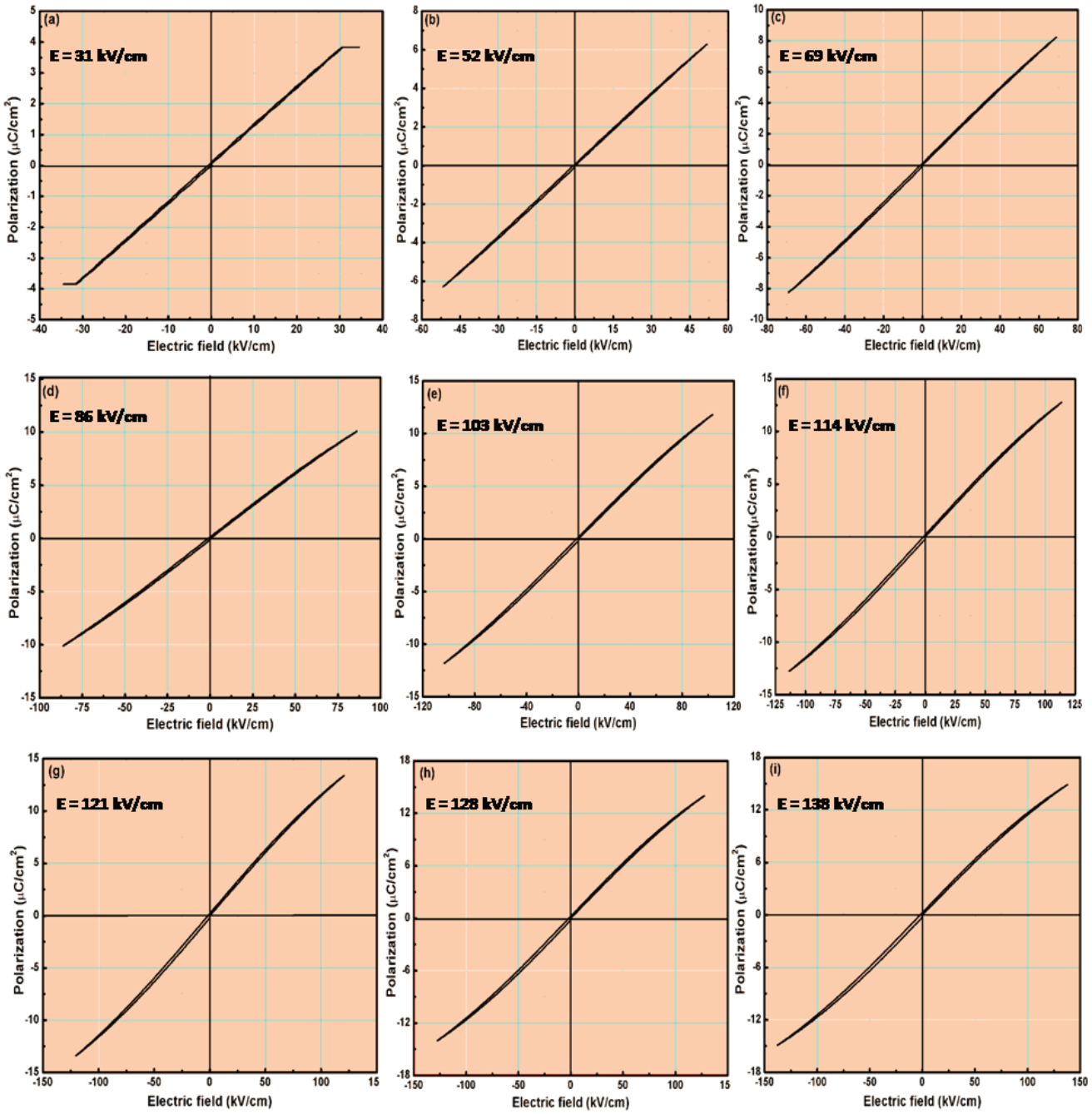

Fig. 5. (a)–(i) Room temperature P–E loops at various electric fields for NBN ceramics.

3. Results and Discussion

The XRD spectrum of NBN ceramic composition sintered at 1275 °C for two hours is shown in Fig. 2. Upon indexing the pattern with standard data, it could be confirmed that the sample comprised a single perovskite phase with no second phase formation within the in-house XRD detection limit. This shows that Bi^{3+} has occupied the Na^{+1} sites in the lattice of NN as its ionic radii ($r_{Bi}{}^{3+} = 1.34$ Å) is matching that of the Na^{+1} ($r_{Na+1} = 1.39$ Å) for coordination no 12.[53] The enlarged XRD pattern of NBN ceramic, in the 2θ range of 32.0–32.6° shows a single (110) peak at 32.4°, and a slight splitting of (200) peak at ~46.4° was also observed, suggesting orthorhombic structure of NBN ceramic system.[54,55] Furthermore the observation of some low intensity peaks marked by arrows around 36–40° may show orthorhombic super structure.

Figure 3(a) shows the secondary electron SEM image (SEI) of the polished and thermally-etched NBN ceramics sample sintered at 1275 °C for two hours. A highly dense

microstructure with almost no porosity can be observed in this image. Nanomeasurer analytical software was used to get grain size distribution, based on which the statistical grain size is measured to be ~0.92 μm, as shown in Fig. 3(b). It has been reported that several microstructural parameters, such as porosity, grain size, second phase formation, and other crystal defects affect the DBS of ceramics.[56] The grain size is considered to mainly affect the DBS of bulk ceramics.[43,57] The smaller grain size of the investigated ceramics is beneficial for DBS and high recoverable energy density. The relationship of DBS to grain size was studied by Tunkasiri *et al*., and is given by the following equation [57]:

$$\mathrm{DBS}\sim\frac{1}{\sqrt{G}}. \tag{4}$$

Figures 4(a) and 4(b) display the variation in dielectric constant (ε_r) and dielectric loss (tanδ) of NBN ceramic with temperature at 1 kHz, 10 kHz, 100 kHz, and 1 MHz. The ε_r graph shows that the investigated ceramics has a Curie temperature below 0 °C, suggesting that NBN belongs to the group II $NaNbO_3$-ABO_3 relaxors. In group II NN-ABO_3 relaxors, the dielectric maximum temperature (T_m) rapidly decreases to a lower temperature region as the ABO_3 end member's concentration increases before reaching a critical value.[58,59] The observed frequency dispersion in ε_r of NBN ceramics may evident relaxor characteristics. The dielectric constants' values at room temperature for NBN ceramics at 1 kHz, 10 kHz, 100 kHz, and 1 MHz were measured to be ~1100, 1080, 1075, and 1060, respectively, accompanied by a low dielectric loss. Upon increasing the temperature, the dielectric loss slightly increased but did not exceed 0.05 up to temperature range of 200 °C at all measured frequencies. The low dielectric loss and the moderate ε_r values are also promising for NBN ceramic's high DBS.[4]

The room temperature P–E loops of NBN ceramics sintered at 1275 °C for two hours at various electric fields are shown in Fig. 5. NBN ceramics display almost linear P–E loops at low electric fields (<70 kV/cm). It exhibits a very

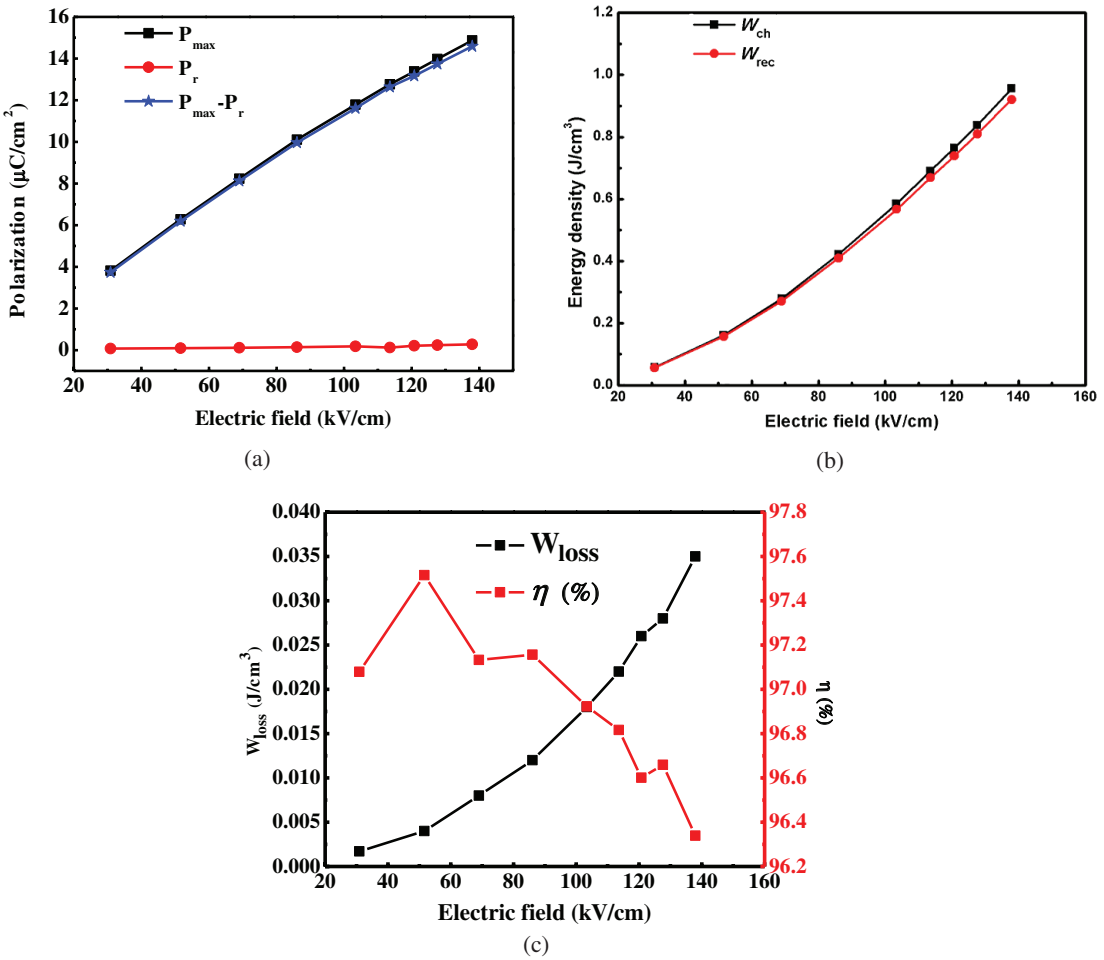

Fig. 6. (a) Variation in P_{max}, P_r, and P_{max}-P_r, (b) energy storage density (W), recoverable energy storage density (W_{rec}), and (c) energy density loss (W_{loss}), and energy storage efficiency (η) of the NBN ceramics at room temperatures as a function of applied electric field.

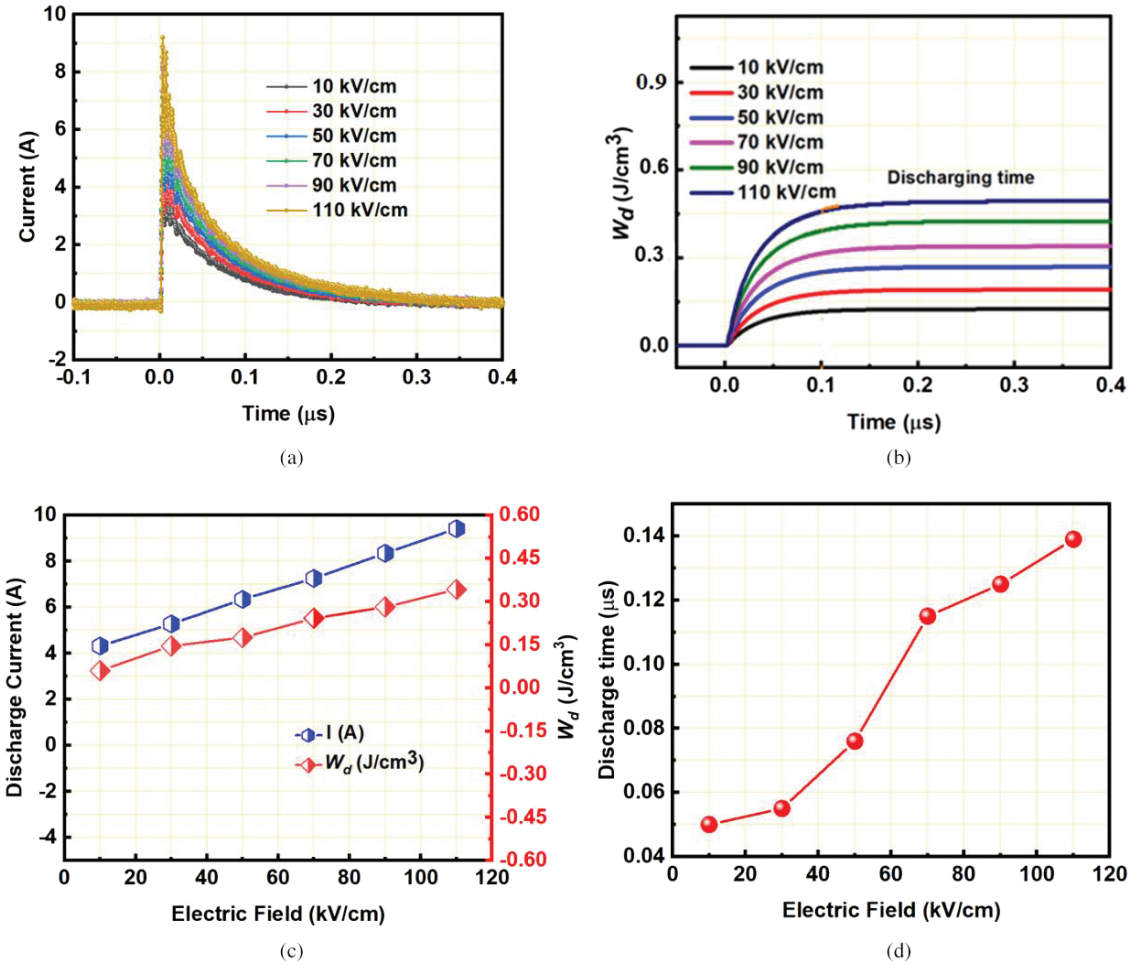

Fig. 7. (a) Variation of the discharge current of NBN ceramics with varying electric fields, (b) relation of W_d and discharge time of NBN ceramics, (c) variation of discharge current and W_d of NBN ceramics, and (d) variation of discharge time of NBN ceramics with the applied electric field.

slight deviation from linearity as the electric field increases to 138 kV/cm. The P–E loops of NBN ceramics possess minimal P_r, slim characteristic and high breakdown strength. Pure NN ceramics has a considerable P_r value showing its ferroelectric nature. Thus, Bi for Na's partial substitution led to lower P_r with a slight decrease in P_{max} and an increase in P_{max}–P_r value. The significantly slimmer P–E loops reflect the typical relaxor characteristic of NBN ceramics. NBN ceramic's relaxor characteristic confirms the existence of polar nano regions (PNRs) where the alignment and back-switching response with electric field is faster for micro-domains than the macroscopic domains. Such a behavior leads to slimmer P–E loops with negligible energy loss.[60] The large P_{max} and nearly zero P_r guarantee large value of W_{rec} and high η, enabling the NBN ceramics to be a good candidate material for energy storage capacitor applications.

Figure 6(a) display the variation in P_{max}, P_r, and P_{max}–P_r's variation of NBN ceramics with applied electric field. The value of P_{max} increased from 3.81 μC/cm^2 to 14.87 μC/cm^2 upon increasing the electric field from 31 kV/cm to the breakdown value of 138 kV/cm. On the other hand, a very small increase in P_r was observed with an increase in the electric field. The P_r's value increased from 0.096 μC/cm^2 to 0.283 μC/cm^2 as the electric field was increased from 31 kV/cm to the breakdown value of 138 kV/cm. Similarly, ΔP (P_{max}–P_r) increased from 3.71 μC/cm^2 to 14.58 μC/cm^2 with an increase in the electric field from 31 kV/cm to 138 kV/cm. The significantly low value of P_r and considerable values of P_{max} and ΔP help in attaining high W_{rec} and η. The values of storage energy density (W_s), the recoverable energy density (W_{rec}) are calculated from the P–E loops of NBN ceramics via Eqs. (1) and (2), while the energy density loss (W_{loss}), and the efficiency (η) are determined via Eq. (3) and are drawn as a function of electric field, as shown in Fig. 5. Upon increasing the electric field from 31 kV/cm to 138 kV/cm, both the energy densities, i.e., W_s and W_{rec} of NBN ceramics increased. Furthermore, with increasing electric field, a slight increase in the energy density loss

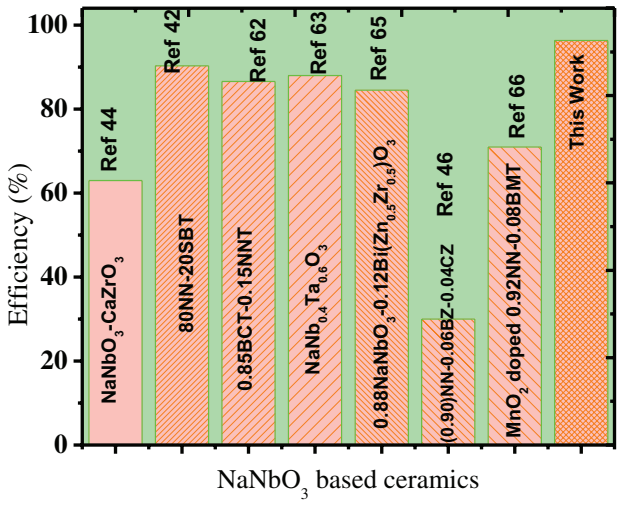

Fig. 8. Comparison of NBN ceramics' energy storage efficiency with some typical lead-free NN ceramics.

accompanied by a slight decrease in the energy storage efficiency was observed. In this study, a high storage energy density (W_s) of 0.96 J/cm^3, a high recoverable energy density (W_{rec}) of 0.92 J/cm^3 accompanied by a high efficiency (η) of 96.33% at DBS of 138 kV/cm were obtained for NBN ceramics.

The discharging rate of the energy by a ceramic capacitor is determined via a discharging experiment, where the measured discharge time ($\tau_{0.9}$) is an important parameter. During this time interval ($\tau_{0.9}$), a capacitor releases ~90% of its discharge energy. The discharged energy density (W_d) and discharged current measured through a load resistance of 1000 Ω at different electric fields of 10 kV/cm, 30 kV/cm, 50 kV/cm, 70 kV/cm, 90 kV/cm, and 110 kV/cm, respectively, for NBN ceramics are shown in Fig. 6.

The discharge energy density (W_d) through this experiment was calculated via the following equation[61]:

$$W_d = R\int i(t)^2 dt/V, \quad (6)$$

where R is the total load resistance (1000 Ω), V is the sample's volume, and $i(t)$ is the discharged current. The measured discharged energy density from the discharged curve via this experiment was less than the recoverable energy density calculated from the P–E loop, as it has been performed at a low electric field (Fig. 7). However, it may also be slightly lower even if measured at the breakdown voltage in this experiment. Two factors are responsible for the lower values of the discharged energy density measured in this experiment. The first factor is the energy losses through the RC circuit, and the second is the variation in the thickness of different samples in the two measurements. The W_d value increased from 0.09 J/cm^3 to 0.4 J/cm^3 as the electric field was increased from 10 kV/cm to 110 kV/cm. The value of $\tau_{0.9}$ increased from 0.05 μs to 0.13 μs when the electric field was increased from 10 kV/cm to 110 kV/cm. This lower discharging time may be may be related to the increased polarization hysteresis with increasing electric field.

The electric-field-dependent (10–110 kV/cm) over damped discharge current curves of NBN ceramic are shown in Fig. 7, in which the current gained the maximum value rapidly in the overall discharge duration (<0.14 μs).

Figure 8 shows a comparison of energy storage efficiency of NBN ceramics to other NN-based ceramics studied previously. It is evident that the energy storage efficiency obtained for NBN ceramic is higher in this study as compared to the previously reported NN-based ceramics.[62–66]

4. Conclusion

Novel single perovskite phase NBN ceramics were successfully synthesized via a solid-state sintering process. In this study, good energy storage density (~0.96 J/cm^3), good recoverable energy density (~0.92 J/cm^3), and high energy storage efficiency (~96.33%) at 138 kV/cm were obtained for the samples investigated in this study. A short pulse discharge time (~0.14 μs) was achieved at room temperature. The results illustrate that NBN ceramics can be a suitable candidate material for energy storage applications as pulsed power ceramic capacitors.

Acknowledgments

The Higher Education Commission (HEC) Islamabad Pakistan has financially supported this work through the National Research Program for University (7488/KPK/NRPU/R&D/HEC/ 2017). The financial support extended by HEC, Pakistan through Project No. NRPU-8148

Conflicts of Interest

There are no conflicts to declare this research work.

References

[1]J. S. Ho and S. G. Greenbaum, Polymer capacitor dielectrics for high temperature applications, *ACS Appl. Mater. Interfaces* **10**, 29189 (2018).
[2]Q. Li, F.-Z. Yao, Y. Liu, G. Zhang, H. Wang and Q. Wang, High-temperature dielectric materials for electrical energy storage, *Ann. Rev. Mater. Res.* **48**, 219 (2018).
[3]Z. Liu, T. Lu, J. Ye, G. Wang, X. Dong, R. Withers and Y. Liu, Antiferroelectrics for energy storage applications: A review, *Adv. Mater. Technol.* **3**, 1800111 (2018).
[4]L. Yang, X. Kong, F. Li, H. Hao, Z. Cheng, H. Liu, J.-F. Li and S. Zhang, Perovskite lead-free dielectrics for energy storage applications, *Prog. Mater. Sci.* **102**, 72 (2019).
[5]X. Hao, J. Zhai and X. Yao, Improved energy storage performance and fatigue endurance of Sr-doped $PbZrO_3$ antiferroelectric thin films, *J. Am. Ceram. Soc.* **92**, 1133 (2009).
[6]L. Jin, F. Li and S. Zhang, Decoding the fingerprint of ferroelectric loops: Comprehension of the material properties and structures, *J. Am. Ceram. Soc.* **97**, 1 (2014).

[7]C. Xu, Z. Liu, X. Chen, S. Yan, F. Cao, X. Dong and G. Wang, High charge-discharge performance of $Pb_{0.98}La_{0.02}(Zr_{0.35}Sn_{0.55}Ti_{0.10})$ 0.995 O_3 antiferroelectric ceramics, *J. Appl. Phys.* **120**, 074107 (2016).
[8]S. Chao, Ceramic dielectrics for high energy density capacity application, *J. Am. Ceram. Soc*. **98**, 1 (2010).
[9]Y. Fu, Y. Wang, S. Wang, Z. Gao and C. Xiong, Enhanced breakdown strength and energy storage of PVDF-based dielectric composites by incorporating exfoliated mica nanosheets, *Polym. Comp*. **40**, 2088 (2019).
[10]X. Xu, W. Liu, Y. Li, Y. Wang, Q. Yuan, J. Chen, R. Ma, F. Xiang and H. Wang, Flexible mica films for high-temperature energy storage, *J. Materiom.* **4**, 173 (2018).
[11]M. Peddigari, H. Palneedi, G.-T. Hwang and J. Ryu, Linear and nonlinear dielectric ceramics for high-power energy storage capacitor applications, *J. Kor. Ceram. Soc.* **56**, 1 (2019).
[12]A. Chauhan, S. Patel, R. Vaish and C. R. Bowen, Anti-ferroelectric ceramics for high energy density capacitors, *Materials* **8**, 8009 (2015).
[13]B. Rangarajan, B. Jones, T. Shrout and M. Lanagan, Barium/lead-rich high permittivity glass–ceramics for capacitor applications, *J. Am. Ceram. Soc.* **90**, 784 (2007).
[14]G. Zhang, D. Zhu, X. Zhang, L. Zhang, J. Yi, B. Xie, Y. Zeng, Q. Li, Q. Wang and S. Jiang, High-energy storage performance of $(Pb_{0.87}Ba_{0.1}La_{0.02})(Zr_{0.68}Sn_{0.24}Ti_{0.08})O_3$ antiferroelectric ceramics fabricated by the hot-press sintering method, *J. Am.Ceram. Soc.* **98**, 1175 (2015).
[15]J. Ge, D. Remiens, X. Dong, Y. Chen, J. Costecalde, F. Gao, F. Cao and G. Wang, Enhancement of energy storage in epitaxial $PbZrO_3$ antiferroelectric films using strain engineering, *Appl. Phys. Lett.* **105**, 112908 (2014).
[16]J. Yi, L. Zhang, B. Xie and S. Jiang, The influence of temperature induced phase transition on the energy storage density of anti-ferroelectric ceramics, *J. Appl. Phys.* **118**, 124107 (2015).
[17]Z. Yang, H. Du, L. Jin, Q. Hu, H. Wang, Y. Li, J. Wang, F. Gao and S. Qu, Realizing high comprehensive energy storage performance in lead-free bulk ceramics via designing an unmatched temperature range, *J. Mater. Chem. A* **7**, 27256 (2019).
[18]Q. Zhang, H. Tong, J. Chen, Y. Lu, T. Yang, X. Yao and Y. He, High recoverable energy density over a wide temperature range in Sr modified (Pb, La)(Zr, Sn, Ti)O_3 antiferroelectric ceramics with an orthorhombic phase, *Appl. Phys. Lett.* **109**, 262901 (2016).
[19]G. Burns and F. Dacol, Glassy polarization behavior in ferroelectric compounds Pb $(Mg_{13}Nb_{23})O_3$ and Pb $(Zn_{13}Nb_{23})O_3$, *Solid State Commun*. **48**, 853 (1983).
[20]W. Huang, Y. Chen, X. Li, G. Wang, N. Liu, S. Li, M. Zhou and X. Dong, Ultrahigh recoverable energy storage density and efficiency in barium strontium titanate-based lead-free relaxor ferroelectric ceramics, *Appl. Phys. Lett.* **113**, 203902 (2018).
[21]D. Zheng, R. Zuo, D. Zhang and Y. Li, Novel $BiFeO_3$–$BaTiO_3$–Ba $(Mg_{1/3}Nb_{2/3})O_3$ lead-free relaxor ferroelectric ceramics for energy-storage capacitors, *J. Am. Ceram. Soc.* **98**, 2692 (2015).
[22]N. Triamnak, R. Yimnirun, J. Pokorny and D. P. Cann, Relaxor characteristics of the phase transformation in $(1–x)$ $BaTiO_{3–x}$Bi $(Zn_{1/2}Ti_{1/2})$ O_3 perovskite ceramics, *J. Am. Ceram. Soc*. **96**, 3176 (2013).
[23]L. Daocheng, D. Shihua, C. Tao and S. Tianxiu, Ferroelectric relaxor behavior of Ba $(Ti_{0.91}Zr_{0.09})O_3$ Ceramics, *Ferroelectrics* **385**, 6169 (2009).
[24]S. Kumaragurubaran, T. Nagata, K. Takahashi, S.-G. Ri, Y. Tsunekawa, S. Suzuki and T. Chikyow, $BaTiO_3$ based relaxor ferroelectric epitaxial thin-films for high-temperature operational capacitors, *Jap. J. Appl. Phy*. **54**, 04DH02 (2015).
[25]T. Wang, L. Jin, C. Li, Q. Hu and X. Wei, Relaxor ferroelectric $BaTiO_3$–Bi $(Mg_{2/3}Nb_{1/3})O_3$ ceramics for energy storage application, *J. Am. Ceram. Soc.* **98**, 559 (2015).
[26]L. Wu, X. Wang and L. Li, Lead-free $BaTiO_3$–Bi $(Zn_{2/3}Nb_{1/3})O_3$ weakly coupled relaxor ferroelectric materials for energy storage, *RSC Adv.* **6**, 14273 (2016).
[27]B. Qu, H. Du and Z. Yang, Lead-free relaxor ferroelectric ceramics with high optical transparency and energy storage ability, *J. Mater. Chem. C* **4**, 1795 (2016).
[28]Z. Yang, H. Du, S. Qu, Y. Hou, H. Ma, J. Wang, J. Wang, X. Wei and Z. Xu, Significantly enhanced recoverable energy storage density in potassium–sodium niobate-based lead free ceramics, *J. Mater. Chem. A* **4**, 13778 (2016).
[29]N. Luo, K. Han, F. Zhuo, L. Liu, X. Chen, B. Peng, X. Wang, Q. Feng and Y. Wei, Design for high energy storage density and temperature-insensitive lead-free antiferroelectric ceramics, *J. Mater. Chem. C* **7**, 4999 (2019).
[30]B. Qu, H. Du, Z. Yang and Q. Liu, Large recoverable energy storage density and low sintering temperature in potassium-sodium niobate-based ceramics for multilayer pulsed power capacitors, *J. Am. Ceram. Soc.* **100**, 1517 (2017).
[31]Y. Tian, L. Jin, H. Zhang, Z. Xu, X. Wei, G. Viola, I. Abrahams and H. Yan, Phase transitions in bismuth-modified silver niobate ceramics for high power energy storage, *J. Mater. Chem. A* **5**, 17525 (2017).
[32]L. Zhao, J. Gao, Q. Liu, S. Zhang and J.-F. Li, Silver niobate lead-free antiferroelectric ceramics: Enhancing energy storage density by B-site doping, *ACS Appl. Mater. Interfaces* **10**, 819 (2018).
[33]Y. Tian, L. Jin, Q. Hu, K. Yu, Y. Zhuang, G. Viola, I. Abrahams, Z. Xu, X. Wei and H. Yan, *J. Mater. Chem. A* **7**, 834 (2019).
[34]N. Luo, K. Han, F. Zhuo, C. Xu, G. Zhang, L. Liu, X. Chen, C. Hu, H. Zhou and Y. Wei, Aliovalent A-site engineered $AgNbO_3$ lead-free antiferroelectric ceramics toward superior energy storage density, *J. Mater. Chem. A* **7**, 14118 (2019).
[35]J. Rödel, K. G. Webber, R. Dittmer, W. Jo, M. Kimura and D. Damjanovic, Transferring lead-free piezoelectric ceramics into application, *J. Eur. Ceram. Soc.* **35**, 1659 (2015).
[36]D. Zheng and R. Zuo, Enhanced energy storage properties in La $(Mg_{1/2}Ti_{1/2})O_3$-modified $BiFeO_3$–$BaTiO_3$ lead-free relaxor ferroelectric ceramics within a wide temperature range, *J. Eur. Ceram. Soc.* **37**, 413 (2017).
[37]J. Roedel and J.-F. Li, Lead-free piezoceramics: Status and perspectives, *MRS Bullet.* **43**, 576 (2018).
[38]Y. Li, N. Sun, J. Du, X. Li and X. Hao, Stable energy density of a PMN–PST ceramic from room temperature to its Curie point based on the synergistic effect of diversified energy, *J. Mater. Chem. C* **7**, 7692 (2019).
[39]F. Wang, C. Ming Leung, Y. Tang, T. Wang and W. Shi, Composition induced structure evolution and large strain response in ternary $Bi_{0.5}Na_{0.5}TiO_3$–$Bi_{0.5}K_{0.5}TiO_3$-$SrTiO_3$ solid solution, *J. Appl. Phys*. **114**, 164105 (2013).
[40]F. Wang, M. Xu, Y. Tang, T. Wang, W. Shi and C. M. Leung, Large strain response in the ternary $Bi_{0.5}Na_{0.5}TiO_3$–$BaTiO_3$–$SrTiO_3$ solid solutions, *J. Am. Ceram. Soc.* **95**, 1955 (2012).
[41]J. Koruza, B. Malič and M. Kosec, Microstructure evolution during sintering of sodium niobate, *J. Am. Ceram. Soc.* **94**, 4174 (2011).
[42]T. Wei, K. Liu, P. Fan, D. Lu, B. Ye, C. Zhou, H. Yang, H. Tan, D. Salamon and B. Nan, Novel $NaNbO_3$–$Sr_{0.7}Bi_{0.2}TiO_3$ lead-free dielectric ceramics with excellent energy storage properties, *Ceram. Int.* **1**, (2020).
[43]A. Xie, H. Qi and R. Zuo, Achieving remarkable amplification of energy-storage density in two step sintered $NaNbO_3$–$SrTiO_3$ antiferroelectric capacitors through dual adjustment of local heterogeneity and grain scale, *ACS Appl. Mater. Interfaces* **12**, 19467 (2020).
[44]Z. Liu, J. Lu, Y. Mao, P. Ren and H. Fan, Energy storage properties of $NaNbO_3$–$CaZrO_3$ ceramics with coexistence of ferroelectric and antiferroelectric phases, *J. Eur. Ceram. Soc.* **38**, 4939 (2018).

[45]R. Shi, Y. Pu, W. Wang, X. Guo, J. Li, M. Yang and S. Zhou, A novel lead-free $NaNbO_3$–Bi $(Zn_{0.5}Ti_{0.5})O_3$ ceramics system for energy storage application with excellent stability, *J. Alloys. Compd.* **815**, 152356 (2020).

[46]W. Tang, Q. Xu, H. Liu, Z. Yao, H. Hao and M. Cao, High energy density dielectrics in lead-free $Bi_{0.5}Na_{0.5}TiO_3$–$NaNbO_3$–Ba $(Zr_{0.2}Ti_{0.8})O_3$ ternary system with wide operating temperature, *J. Mater. Sci.: Mater. Electron.* **27**, 6526 (2016).

[47]F. Yan, H. Yang, Y. Lin and T. Wang, Dielectric and ferroelectric properties of $SrTiO_3$–$Bi_{0.5}Na_{0.5}TiO_3$–$BaAl_{0.5}Nb_{0.5}O_3$ lead-free ceramics for high-energy-storage applications, *Inorg. Chem.* **56**, 13510 (2017).

[48]A. Zeb and S. Milne, High temperature dielectric ceramics: A review of temperature-stable high-permittivity perovskites, *J. Mater. Sci.: Mater. Electron.* **26**, 9243 (2015).

[49]L. Luo, B. Wang, X. Jiang and W. Li, Energy storage properties of $(1-x)(Bi_{0.5}\ Na_{0.5})TiO_{3-x}KNbO_3$ lead-free ceramics, *J. Mater. Sci.* **49**, 1659 (2014).

[50]B. Wang, L. Luo, X. Jiang, W. Li and H. Chen, Energy-storage properties of $(1-x)$ $Bi_{0.47}Na_{0.47}Ba_{0.06}TiO_{3-x}KNbO_3$ lead-free ceramics, *J. Alloys. Compd.* **585**, 14 (2014).

[51]F. Gao, X. Dong, C. Mao, F. Cao and G. Wang, c/a Ratio-dependent energy-storage density in $(0.9-x)$ $Bi_{0.5}Na_{0.5}TiO_{3-x}BaTiO_{3-0.1}$-$K_{0.5}Na_{0.5}NbO_3$ Ceramics, *J. Am. Ceram. Soc.* **94**, 4162 (2011).

[52]H. Borkar, V. Singh, B. Singh, M. Tomar, V. Gupta and A. Kumar, Room temperature lead-free relaxor–antiferroelectric electroceramics for energy storage applications, *RSC Adv.* **4**, 22840 (2014).

[53]R. D. Shannon, Revised effective ionic radii and systematic studies of interatomic distances in halides and chalcogenides, *Acta Crystallograph. A: Cryst. Phy. Diff. Theor. Gen.crystall.* **32**, 751 (1976).

[54]J. Shi, X. Chen, C. Sun, F. Pang, H. Chen, X. Dong, X. Zhou, K. Wang and H. Zhou, Enhanced energy storage performance of sodium niobate-based relaxor dielectrics by a ramp-to-spike sintering profile, *Ceram. Int*. **46**, 25737 (2020).

[55]Z. Yang, H. Du, L. Jin, Q. Hu, S. Qu, Z. Yang, Y. Yu, X. Wei and Z. Xu, A new family of sodium niobate-based dielectrics for electrical energy storage applications, *J. Eur. Ceram. Soc.* **39**, 2899 (2019).

[56]Z. Yao, Z. Song, H. Hao, Z. Yu, M. Cao, S. Zhang, M. T. Lanagan and H. Liu, Homogeneous/inhomogeneous-structured dielectrics and their energy-storage performances, *Adv. Mater.* **29**, 1601727 (2017).

[57]Z. Yang, F. Gao, H. Du, L. Jin, L. Yan, Q. Hu, Y. Yu, S. Qu, X. Wei and Z. Xu, Grain size engineered lead-free ceramics with both large energy storage density and ultrahigh mechanical properties, *Nano Energy* **58**, 768 (2019).

[58]L. Yang, X. Kong, Z. Cheng and S. Zhang, Enhanced energy density and electric cycling reliability via MnO_2 modification in sodium niobate-based relaxor dielectric capacitors, *J. Mater. Res.* **1**, 899 (2019).

[59]I. Raevski and S. Prosandeev, A new, lead free, family of perovskites with a diffuse phase transition: $NaNbO_3$-based solid solutions, *J. Phy. Chem. Solid.* **63**, 1939 (2002).

[60]N. Qu, H. Du and X. Hao, A new strategy to realize high comprehensive energy storage properties in lead-free bulk ceramics, *J. Mater. Chem. C* **7**, 7993 (2019).

[61]F. Li, K. Yang, X. Liu, J. Zou, J. Zhai, B. Shen, P. Li, J. Shen, B. Liu and P. Chen, Temperature induced high charge–discharge performances in lead-free $Bi_{0.5}Na_{0.5}TiO_3$-based ergodic relaxor ferroelectric ceramics, *Scrip. Mater.* **141**, 15 (2017).

[62]A. Jain, Y. Wang and H. Guo, Microstructural properties and ultrahigh energy storage density in $Ba_{0.9}Ca_{0.1}TiO_3$–$NaNb_{0.85}Ta_{0.15}O_3$ relaxor ceramics, *Ceram. Int.* **46**, 24333 (2020).

[63]J. Bian, M. Otonicar, M. Spreitzer, D. Vengust and D. Suvorov, Structural evolution, dielectric and energy storage properties of $Na(Nb_{1-x}Tax)O_3$ ceramics prepared by spark plasma sintering, *J. Eur. Ceram. Soc.* **39**, 2339 (2019).

[64]J. Shi, X. Chen, C. Sun, F. Pang, H. Chen, X. Dong, X. Zhou, K. Wang and H. Zhou, Superior thermal and frequency stability and decent fatigue endurance of high energy storage properties in $NaNbO_3$-based lead-free ceramics, *Ceram. Int.* **46**, 25731 (2020).

[65]H. Qi, R. Zuo, A. Xie, J. Fu and D. Zhang, Excellent energy-storage properties of $NaNbO_3$-based lead-free antiferroelectric orthorhombic P-phase (Pbma) ceramics with repeatable double polarization-field loops, *J. Eur. Ceram. Soc.* **39**, 3703 (2019).

[66]A. Tian, R. Zuo, H. Qi and M. Shi, Large energy-storage density in transition-metal oxide modified $NaNbO_3$–Bi $(Mg_{0.5}Ti_{0.5})O_3$ lead-free ceramics through regulating the antiferroelectric phase structure, *J. Mater. Chem. A* **8**, 8352 (2020).